Vol 15 No 9, September 2006
1009-1963/2006/15(09)/2058-07

Chinese Physics

© 2006 Chin. Phys. Soc.
and IOP Publishing Ltd

X-ray observations of tungsten wire array Z-pinch implosions on QiangGuang-1 facility*

Zhang Fa-Qiang(章法强)[a)b)†], Li Zheng-Hong(李正宏)[b)], Xu Ze-Ping(许泽平)[b)], Xu Rong-Kun(徐荣昆)[b)], Yang Jian-Lun(杨建伦)[b)], Guo Cun(郭 存)[b)], Xia Guang-Xin(夏广新)[b)], Chen Jin-Chuan(陈进川)[b)], Song Feng-Jun(宋凤军)[b)], Ning Jia-Min(宁家敏)[b)], Wang Zhen(王 真)[b)], Xue Fei-Biao(薛飞彪)[b)], Li Lin-Bo(李林波)[b)], Qin Yi(秦 义)[b)], Ying Chun-Tong(应纯同)[a)], and Liu Guang-Jun(刘广均)[a)]

[a)] *Department of Engineering Physics, Tsinghua University, Beijing* 100084, *China*

[b)] *Institute of Nuclear Physics and Chemistry, Mianyang* 621900, *China*

(Received 16 November 2005; revised manuscript received 18 May 2006)

Z-pinch experiments with two arrays consisting, respectively, of 32 4-μm- and 6-μm-diameter tungsten wires have been carried out on QiangGuang-1 facility with a current rising up to 1.5 MA in 80 ns. At early time of implosion, x-ray framing images show that the initial emission comes from the central part of arrays, and double clear emission rings, drifting to the anode and the cathode at 5×10^6 cm/s and 2.4×10^7 cm/s respectively, are often produced near the electrodes. Later, in a 4-μm-diameter tungsten wire array, filamentation caused by ohmic heating is prominent, and more than ten filaments have been observed. A radial inward shift of arrays starts at about 30 ns earlier than the occurrence of the x-ray peak power for both kinds of arrays, and the shrinkage rate of emission region is as high as 1.7×10^7 cm/s in a 4-μm-diameter tungsten wire array, which is two times higher than that in a 6-μm one. Emission from precursor plasmas is observed in implosion of 6-μm-diameter tungsten wire arrays, but not in implosion of a 4-μm-diameter tungsten wire array. Whereas, in a 4-μm-diameter tungsten wire array, the soft x-ray emission shows the growth of m=1 instability in the plasma column, which is caused by current. The reasons for the discrepancy between implosions of 4-μm- and 6-μm-diameter tungsten wire arrays are explained.

Keywords: Z-pinch, x-ray, wire array, $R-T$ instability
PACC: 5255E, 5270L, 5255M

1. Introduction

Wire array Z-pinches driven by pulsed-power generators are intense x-ray sources,[1,2] which have important applications in inertial confinement fusions[2−4] and other high energy density studies.[5,6] According to a heuristic model,[7] the process of Z-pinch implosion includes plasma expanding with uncorrelated magnetohydrodynamic (MHD) instability, plasma merging caused by the global magnetic field, inward acceleration of the shell and stagnation at the axis with intense x-ray emission.[8,9] The x-ray peak power and pulse duration are greatly suppressed by the development of Rayleigh–Taylor ($R-T$) instability. To enhance the implosion efficiency of Z-pinches, a lot of attempts have been made to mitigate the $R-T$ instability by improving the uniformity and symmetry of pinch loads. For instance, using a nested array of fine tungsten wires, the researchers at Sandia National Laboratories achieved 2MJ of soft x-ray in a 5-ns pulse with a peak power of 280TW on the Z-machine driven by a 20-MA current rising in about 80 ns.[10,11] At the same time, in experiments on the generators driven by small currents, such as the MAGPIE generator (1.4 MA in 240 ns) and QiangGuang-1 facility (1.5 MA in 80 ns), much attention has been paid to the plasma formation and implosion dynamics.[12−17]

To investigate the implosion dynamics of tungsten wire array Z-pinch and the characteristics of x-ray emission, we perform the experiments on QiangGuang-1 facility, which has a storage energy of up to 260 kJ and can deliver about 80 kJ into pinch loads in 80 ns with a discharge current of up to 1.6 MA.[18] The experimental results show that the development of instability is very dissimilar to that in the implosion of arrays with different parameters.

*Project supported by the National Natural Science Foundation of China (Grant No 10035030).
†E-mail: zhangfaqiang@tsinghua.org.cn

2. Experimental setup

In our experiments, two arrays consisting, respectively, of 32 4-μm- and 6-μm-diameter tungsten wires were arranged into a 4-mm-radius circle and located between electrodes with a 20-mm separation in between. The experimental arrangement is depicted in Fig.1. In order to study implosion process, a set of diagnostic equipments were employed. A time-resolved pinhole camera (2-ns gate time with a 10-ns interval) was used to obtain soft x-ray images, which was filtered by a 2-μm polypropylene foil and was sensitive to 100 eV–10 keV photons. The x-ray emission bursts were recorded by an x-ray power meter (XRPM).[19,20] Time-integrated images were obtained by pinhole cameras with different filters.

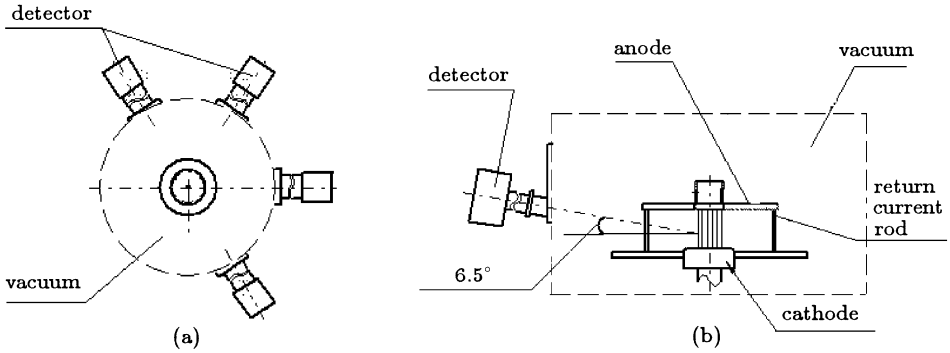


Fig.1. Schematic of experiment arrangement. (a) the $r-\theta$ plane and (b) the $r-z$ plane.

3. Experimental results and analysis

Figure 2 displays the soft x-ray emission during the implosion of a 4-μm-diameter tungsten wire array. Part of the image at +14.7 ns is blocked. The initial emission comes from the central part of the array and two elliptical rings appear in the figure. Considering the 6.5° viewing angle shown in Fig.1(b), one can confirm that the elliptical shapes of rings are corresponding projections of the circles in the $r-\theta$ plane.

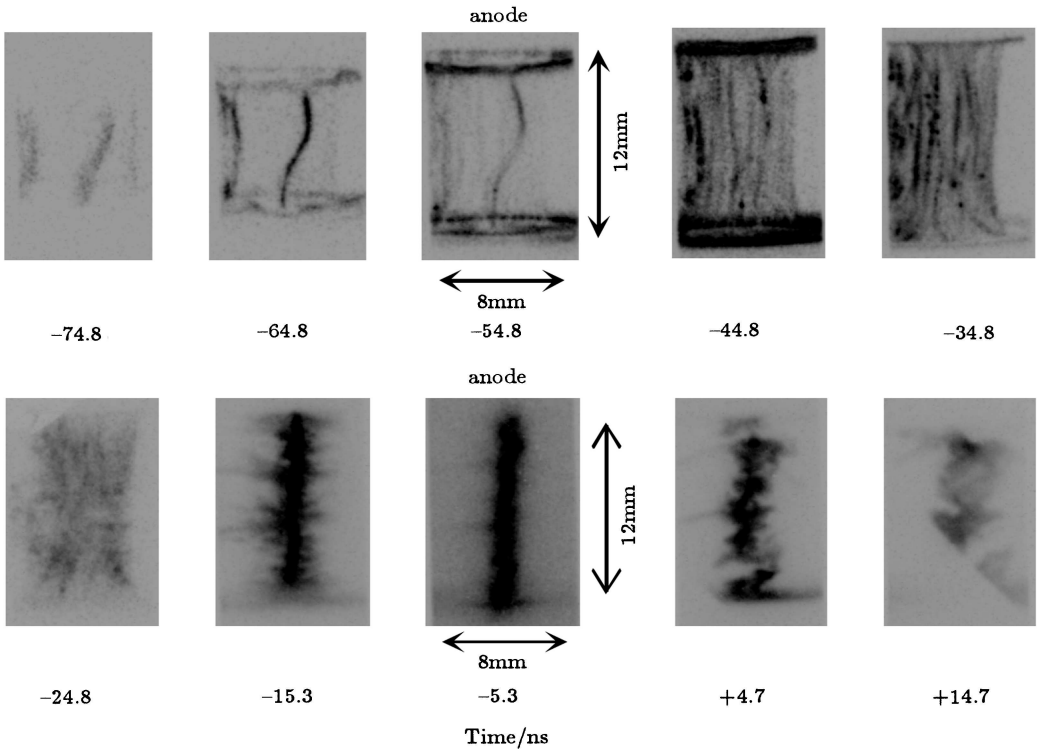


Fig.2. X-ray pinhole time-resolved camera images of shot 04154. Diameter of the pinhole in the first five images is $\phi 100\pm 10\mu$m, and $\phi 30\pm 1\mu$m in the remaining. Time below each image is measured with respect to the time of peak power measured in XRPM.

The near-cathode emission ring drifts to the cathode at an average rate dropping from about 2.4×10^7 cm/s between –64.8 ns and –54.8 ns, to about 1.5×10^7 cm/s between –54.8 ns and –44.8 ns. Meanwhile, the near-anode ring drifts to the opposite side only at one-third of the rate. As shown in the figure, filamentation is prominent at –44.8 ns and –34.8 ns and more than ten filaments come into view. Later, the emission region shrinks at an average rate of about 1.7×10^7 cm/s between –24.8 ns and –15.3 ns, which is worked out from Fig.3. The global $R-T$ instability has a characteristic wavelength of $\lambda\approx0.4$ mm at –24.8 ns, and 10 ns later it develops to $\lambda\approx0.7$ mm (Fig.4). At –15.3 ns, the size of emission region is 1.6×13 mm^2, and a 5-to-1 radial convergence is estimated here. The image at –5.3 ns shows an m=1 instability with a spatial period of about 2.2 mm∼2.4 mm, which can be clearly seen in Fig.5 after the image is processed.

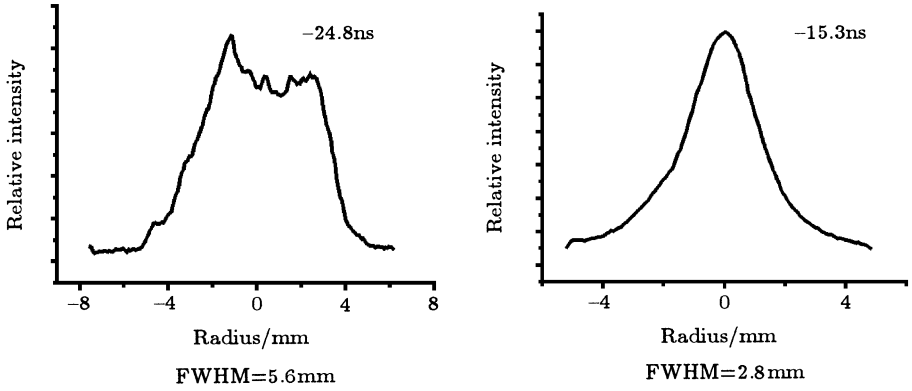


Fig.3. Radial profiles of two images shown in Fig.2 that are integrated over the z-axis.

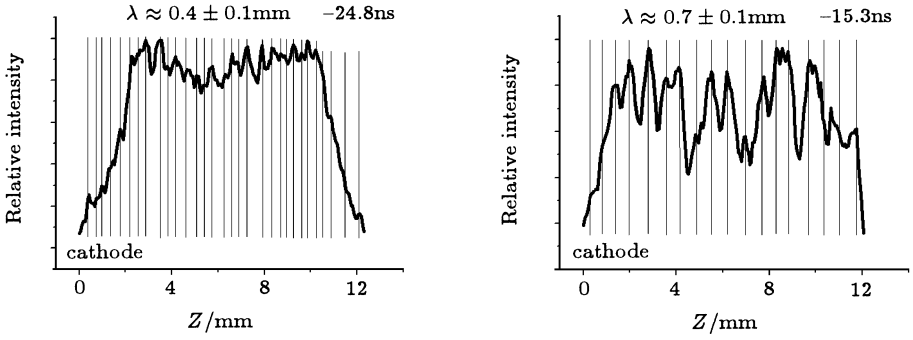


Fig.4. Axial profiles of two images shown in Fig.2 that are integrated over the r-axis for a local area.



Fig.5. The image showing an m=1 instability with a wavelength of 2.2 mm≈ 2.4 mm at –5.3 ns in a 4-μm tungsten wire array.

The implosion of an array of 6-μm-diameter tungsten wires is shown in Fig.6. Because of the smaller pinholes, the images before –30 ns are lighter than those of shot 04154, and the near-cathode emission ring is weak at –60.5 ns. The soft x-ray emission of precursor plasma is observed at –40.5 ns and at –30.5 ns, and the precursor plasma appears to be elongated along the z-axis to the cathode at an average rate of about 3.5×10^7 cm/s. The emission region shrinks at a rate of about 8×10^6 cm/s between –20.5 ns and –11 ns (Fig.7). At –20.5 ns, the global $R-T$ instability has a characteristic wavelength of 0.7 mm, which develops to 1.3 mm at –11 ns (Fig.8). At –1 ns, the size

of emission region is 1.9 mm×13 mm, and the radial convergence is estimated to be 4.2 here.

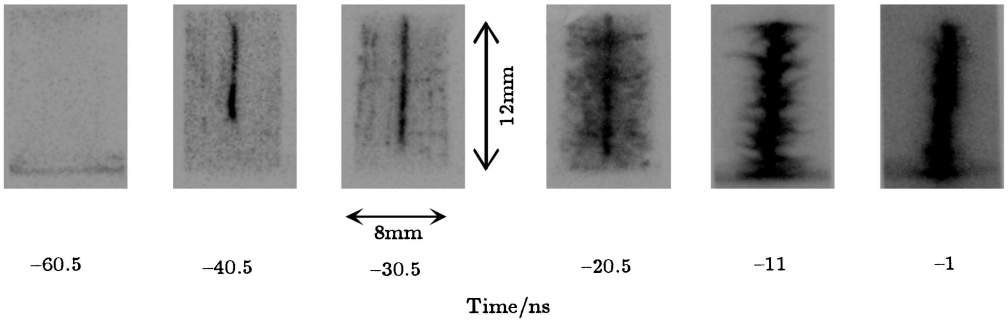


Fig.6. X-ray pinhole time-resolved camera images of shot 04153. Diameter of the pinhole in the first three images is $\phi 45\pm 5\mu$m, and $\phi 30\pm 1\mu$m in the remaining. Time below each image is measured with respect to time of peak power measured in XRPM.

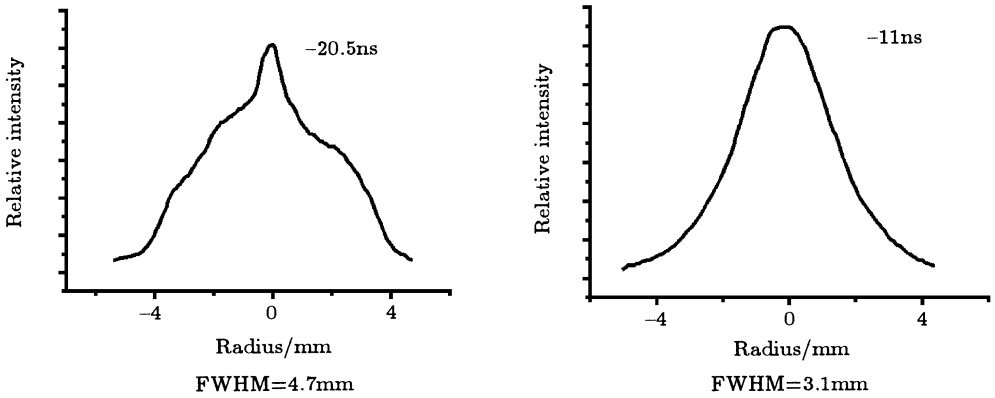


Fig.7. Radial profiles of two images shown in Fig.6 that are integrated over the z-axis.

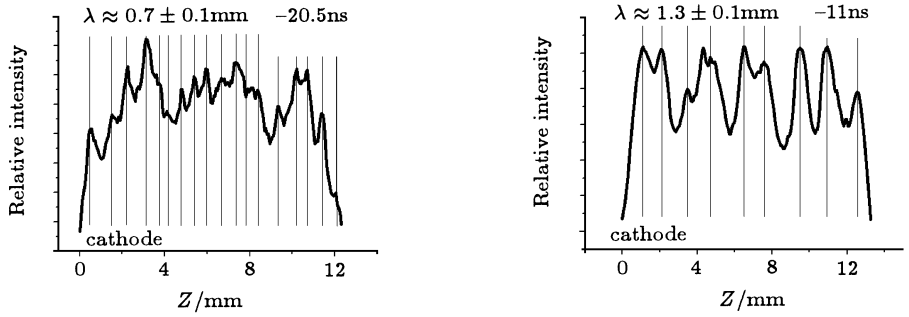


Fig.8. Axial profiles of two images shown in Fig.6 that are integrated over the r-axis for a local area.

Figure 9 shows images obtained by the time-integrated x-ray pinhole cameras with different filters. The camera filtered by a 5-μm Al foil was sensitive to 800 eV–1500 eV photons and had an aperture of 5 μm. The camera filtered by a 100-μm Ti foil and a 1-mm Al foil was sensitive to photons greater than 10 keV, and because of an aperture of 1 mm, the camera could obtain only shadow images because of relatively large visual angle for a small hard x-ray emission region. The images indicate that there exists hard x-ray emission in shot 04153, but not in shot 04154.

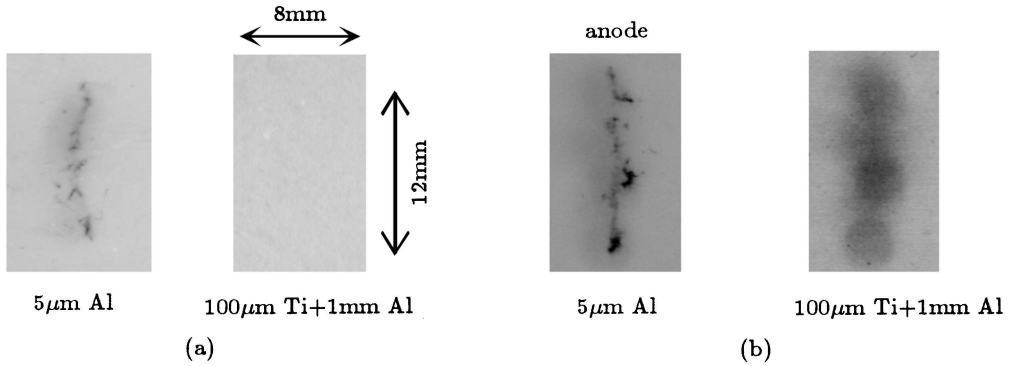


Fig.9. Time-integrated x-ray pinhole images of shot 04154 (a) and shot 04153 (b). Below images indicated are the materials of the filters and their thickness.

4. Discussion

In the experiments, the initial emission from plasmas is often observed to appear at the central part of an array, and with double emission rings drifting to electrodes respectively, the region of emission extends to the whole array (as shown in Fig.2). The near-cathode emission circle drifts to the cathode at a typical rate of $(2\pm0.5)\times10^7$ cm/s, while the near-anode one at a rate two times slower than the former. The mechanism of the generation of emission rings and their behaviours needs further study.

The average implosion time is defined as the phase time from the start of currents to occurrence of peak power measured by XRPM. Two kinds of arrays exhibit variant implosion times. The implosion time is on average 20 ns shorter in a 4-μm-diameter tungsten wire array than in a 6-μm one (as shown in Fig.10). On the other hand, obvious radial inward shifts of both arrays begin at about 30 ns earlier than the occurrence of the x-ray peak power measured by XRPM. This means that the ablation of wires into plasma in a 4-μm-diameter tungsten wire array takes a shorter time than in a 6-μm one. Obviously, this results from the smaller line mass density (78μg/cm) in a 4-μm-diameter wire array. It seems that ablation rates of the wires in both kinds of arrays are identical. However, implosions of both arrays take almost the same time of 30 ns from the start of shrinkage to the x-ray peak power.

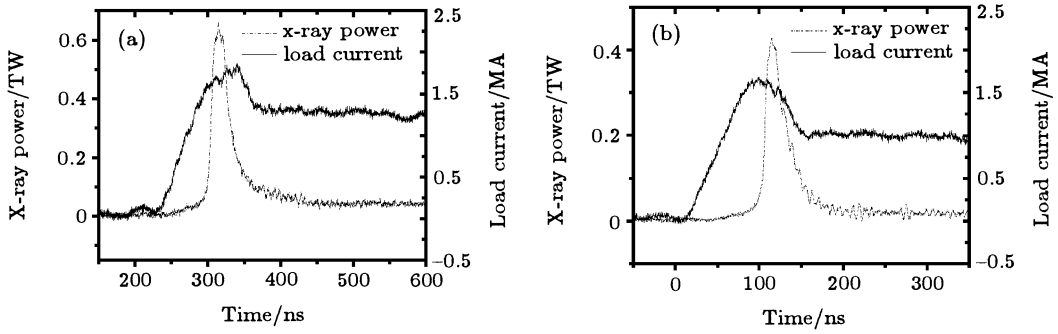


Fig.10. Typical waveforms of load current together with the waveforms of x-ray power measured by XRPM. (a) 4-μm-diameter tungsten wire array, (b) 6-μm-diameter tungsten wire array.

For the different arrays, the developments of instabilities show different characters. In the implosion of a 4-μm-diameter tungsten wire array, filamentation is prominent, and this is caused by ohmic heating which leads to an azimuthal instability.[21] When the plasma exerted by a force $\boldsymbol{J}\times\boldsymbol{B}$ converges to the axis and a plasma column comes into being, the current passing through it is still rising up and lasts a relatively long time. This leads to an obvious m=1 instability as shown in Fig.5. However, the scenario is not exactly the same in the implosion of a 6-μm-diameter tungsten wire array. On initiation, wires are ablated into plasma corona due to ohmic heating, and the current passes through the corona. Being exerted

by $\boldsymbol{J} \times \boldsymbol{B}$, a fraction of corona plasma begins to converge to the axis, and an observable precursor plasma is gradually formed (as shown in Fig.6). Meanwhile, dense cores of wires are still heated by thermal conduction from the hot plasma corona. This phase lasts 20 ns that is longer than that in a 4-μm-diameter tungsten wire array. In this longer time, $R-T$ instability develops on a larger scale ($\lambda \approx 0.7$ mm at –20.5 ns, $\lambda \approx 1.3$ mm at -11 ns), hence, it is fiercer than in a 4-μm-diameter tungsten wire array. Owing to the sufficient development of $R-T$ instability, the average imploding rate is much slower and a smaller radial convergence is gained than in implosions of a 4-μm-diameter tungsten wire array.

The time-integrated x-ray pinhole images show that bright spots are distributed along a distorted line in shot 04154 (a 4-μm-diameter tungsten wire array), and there is no hard x-ray emission observed. While in shot 04153 (a 6-μm-diameter tungsten wire array), a majority of bright spots are distributed along a straight line, and there are three spots where the emission of hard x-ray (above 10 keV) takes place. These suggest that when the plasma column is formed on the z-axis, the kink instability is noticeable and its development achieves a vicious twist on the column in a 4-μm-diameter tungsten wire array, which destroys the ideal pinch of the column and baffles the generation of hard x-ray. This is consistent with the analyses in the above sections.

5. Conclusions

The implosions of two arrays consisting, respectively, of 32 4-μm- and 6-μm-diameter tungsten wires show dissimilar characters on QiangGuang-1 facility. In a 4-μm-diameter tungsten wire array, the smaller line density leads to an obvious filamentation and a relatively fast implosion, during which the $R-T$ instability is suppressed effectively and a higher implosion rate is obtained. Meanwhile, an m=1 instability takes place on the plasma column before the occurrence of x-ray peak power, and this destroys a preferable pinch of plasma. Whereas, in a 6-μm-diameter tungsten wire array, the ablation of wires into plasma takes longer time and precursor plasma appears at the axis. Hence, the global $R-T$ instability develops fiercely and leads to a humble implosion rate and a modest radial convergence. It seems that the array consisting of 4-μm- or 6-μm-diameter tungsten wires is not optimal. Compared with the previous work,[18] we conclude that, in the sense of x-ray power and yield, arrays with moderate parameters, such as a 5-μm-diameter tungsten wire array, are optimal for QiangGuang-1 facility.

References

[1] Baker K L, Porter J L, Ruggles L E, Chandler G A, Deeney C, Vargas M, Moats A, Struve K, Torres J, McGurn J, Simpson W W and Fehl D L 1999 *Appl. Phys. Lett.* **75** 775

[2] Matzen M K, Deeney C, Leeper R J, Porter J L, Spielman R B, Chandler G A, Derzon M S, Douglas M R, Fehl D L, Hebron D E, Nash T J, Olson R E, Ruggles L E, Sanford T W L, Seamen J F, Struve K W, Stygar W A and Peterson D L 1999 *Plasma Phys. Control. Fusion* **41** A 175

[3] Bennett G R, Vesey R A, Cuneo M E, Porter J L, Adams R G, Aragon R A, Rambo P K, Rovang D C, Ruggles L E, Simpson W W, Smith I C, Speas C S, Struvee K W and Wenger D F 2003 *Phys. Plasmas* **10** 3717

[4] Sanford T W L, Lemke R W, Mock R C and Peterson D L 2003 *Phys. Plasmas* **10** 3252

[5] Hu M and Kusse B R 2004 *Phys. Plasmas* **11** 1145

[6] Deeney C, Coverdale C A, Douglas M R, Nash T J, Spielman R B, Struve K W, Whitney K G, Thornhill J W, Apruzese J P, Clark R W, Davis J, Beg F N and Ruiz-Camacho J 1999 *Phys. Plasmas* **6** 2081

[7] Hussey T W, Roderick N F, Shumlak U, Spielman R B and Deeney C 1995 *Phys. Plasmas* **2** 2055

[8] Lebedev S V, Beg F N, Bland S N, Chittenden J P, Dangor A E, Haines M G, Pikuz S A and Shelkovenko T A 2000 *Phys. Rev. Lett.* **85** 98

[9] Beg F N, Ruiz Camacho J, Haines M G and Dangor A E 2004 *Plasma Phys. Control. Fusion* **46** 1

[10] Spielman R B, Deeney C, Chandler G A, Douglas M R, Fehl D L, Matzen M K, McDaniel D H, Nash T J, Porter J L, Sanford T W L, Seamen J F, Stygar W A, Struve K W, Breeze S P, McGurn J S, Torres J A, Zagar D M, Gilliland T L, Jobe D O, McKenney J L, Mock R C, Vargas M, Wagoner T and Peterson D L 1998 *Phys. Plasmas* **5** 2105

[11] Deeney C, Douglas M R, Spielman R B, Nash T J, Peterson D L, L'Eplattenier L, Chandler G A, Seamen J F and Struve K W 1998 *Phys. Rev. Lett.* **81** 4883

[12] Lebedev S V, Beg F N, Bland S N, Chittenden J P, Dangor A E, Haines M G, Kwek K H, Pikuz S A and Shelkovenko T A 2001 *Phys. Plasmas* **8** 3734

[13] Zeng Z Z and Qiu A C 2004 *Chin. Phys.* **13** 201

[14] Duan Y Y, Guo Y H, Wang W S and Qiu A C 2005 *Chin. Phys.* **14** 1856

[15] Ding N, Yang Z H and Ning C 2004 *Acta Phys. Sin.* **53** 808 (in Chinese)

[16] Duan Y Y, Guo Y H, Wang W S and Qiu A C 2004 *Acta Phys. Sin.* **53** 2654 (in Chinese)

[17] Duan Y Y, Guo Y H, Wang W S and Qiu A C 2004 *Acta Phys. Sin.* **53** 3429 (in Chinese)

[18] Xu R K, Li Z H, Yang J L, Xu Z P, Ding N, Guo C, Jiang S L, Ning J M, Xia G X, Li L B, Song F J and Cheng J C 2005 *Chin. Phys.* **14** 1613

[19] Xu R K, Li Z H, Ning J M, Guo C, Xu Z P, Yang J L, Li L B, Xia G X, Hua X S, Ding N, Liu Q, Gu Y C, Grabovsky E V, Oleynic G M, Nedoseev S L, Alexandrov V V, Mitrofanov K N, Zurin M V, Volkov G S, Porofeev I A, Frolov I N and Smirnov V P 2005 *Chin. Phys. Lett.* **22** 413

[20] Guo C, Xu R K, Lee Z H, Xia G X, Ning J M and Song F J 2004 *Acta Phys. Sin.* **53** 1331 (in Chinese)

[21] Liberman M A, De Groot J S, Toor A and Spielman R B 1999 *Physics of High-Density Z-Pinch Plasmas* (New York: Springer) pp115–118